

Article

The Influence of Fracturing Fluid Volume on the Productivity of Coalbed Methane Wells in the Southern Qinshui Basin

Wenwen Chen ¹, Xiaoming Wang ^{1,*}, Mingkai Tu ¹, Fengjiao Qu ², Weiwei Chao ³, Wei Chen ⁴ and Shihui Hou ⁵

¹ Key Laboratory of Tectonics and Petroleum Resources, China University of Geosciences, Wuhan 430074, China

² Engineering Technology Research Institute, PetroChina Huabei Oilfield Company, Renqiu 062550, China

³ China United Coalbed Methane Company Limited, Taiyuan 030000, China

⁴ CBM Exploration and Development Branch, PetroChina Huabei Oilfield Company, Jincheng 047000, China

⁵ Laboratory of Geotechnical Engineering, Jingtangshan University, Ji'an 343000, China

* Correspondence: sunwxm@cug.edu.cn

Abstract: Hydraulic fracturing is the main technical means for the reservoir stimulation of coalbed methane (CBM) vertical wells. The design of fracturing fluid volume (FFV) is mainly through numerical simulation, and the numerical simulation method does not fully consider the water block damage caused by the leakage of fracturing fluid into the reservoir. In this work, the variance analysis method was used to analyze the production data of 1238 CBM vertical wells in the Fanzhuang block and Zhengzhuang block of the Qinshui Basin, to clarify the relationship between the FFV and the peak gas production (PGP) under the different ratios of critical desorption pressure to reservoir pressure ($R_{c/r}$), and to reveal the controlling mechanism of fracturing fluid on CBM migration. The results show that both the FFV and $R_{c/r}$ have a significant impact on gas production. When $R_{c/r} < 0.5$, the PGP decreases with the increase of the FFV, and the FFV that is beneficial to gas production is 200–500 m³. When $R_{c/r} > 0.5$, the PGP increases first and then decreases with the increase of FFV. Specifically, the FFV that is favorable for gas production is 500–700 m³. Excessive FFV does not significantly increase the length of fractures due to leaks in the coal reservoir. Instead, it is more likely to invade and stay in smaller pores, causing water block damage and reducing gas production. Reservoirs with high $R_{c/r}$ have larger displacement pressure, which can effectively overcome the resistance of liquid migration in pores, thereby reducing the damage of the water block. Therefore, different reservoir conditions need to match the appropriate fracturing scale. This study can provide guidance for the optimal design of hydraulic fracturing parameters for CBM wells.

Keywords: coalbed methane; hydraulic fracturing; fracturing fluid volume; analysis of variance; water block



Citation: Chen, W.; Wang, X.; Tu, M.; Qu, F.; Chao, W.; Chen, W.; Hou, S. The Influence of Fracturing Fluid Volume on the Productivity of Coalbed Methane Wells in the Southern Qinshui Basin. *Energies* **2022**, *15*, 7673. <https://doi.org/10.3390/en15207673>

Academic Editor: Mohammad Sarmadivaleh

Received: 22 September 2022

Accepted: 14 October 2022

Published: 18 October 2022

Publisher's Note: MDPI stays neutral with regard to jurisdictional claims in published maps and institutional affiliations.



Copyright: © 2022 by the authors. Licensee MDPI, Basel, Switzerland. This article is an open access article distributed under the terms and conditions of the Creative Commons Attribution (CC BY) license (<https://creativecommons.org/licenses/by/4.0/>).

1. Introduction

Hydraulic fracturing is one of the important reservoir stimulations of coalbed methane (CBM) wells, and its main purpose is to form efficient conductivity fractures and improve coal seam permeability [1,2]. However, while hydraulic fracturing improves the permeability of coal seams, tons of fracturing fluid are injected into the coal seam [3,4], and a large amount of fracturing fluid is leaked into the coal reservoir, which also brings many adverse effects to the development of coalbed methane, such as water block damage [5–8], clay swelling [9,10], and consequently increased difficulty in methane desorption, etc. [11,12].

In view of the adverse effects of fracturing fluid leakage, a large number of scientific research and experiments have been carried out on the influencing factors of the leakage. Yuan et al. [4] and Chang et al. [10] studied the self-absorption process and microscopic migration mechanism of coal reservoirs after hydraulic fracturing and evaluated the effect of this process on permeability. Wang et al. [13] expounded the influence of the wettability of coal on the irreducible water content from a microscopic point of view, and discussed

the effective flowback of fracturing fluid after hydraulic fracturing. Meng et al. [14] studied the effects of effective stress, porosity, permeability, fracturing fluid viscosity, and reservoir pressure on the fracturing fluid leakage factor, and proposed a model that takes into account stress-sensitivity effects to estimate the overall filter leakage factor. Through numerical simulation, Guo et al. [15] showed that fracture geometry, reservoir characteristics, pressure conditions, and temperature have significant effects on fracturing fluid leakage. Guo et al. [16] observed that natural fractures play a dominant role in the leak of fracturing fluid, and the wider the opening of natural fractures, the greater the leak of fracturing fluid. From the perspective of fracturing engineering, Wu et al. [17] showed through experimental results that increasing the injection pressure will increase the fracturing fluid loss; true triaxial hydraulic fracturing experiments showed that high injection rates can cause a large amount of fracturing fluid to leak along the bedding direction [18]. However, the unreasonable fracturing scale design may also be the root cause for fracturing fluid leakage, which has rarely attracted the attention of scholars.

The design of FFV needs to consider different reservoir conditions. The appropriate fracturing fluid scale can not only achieve the maximum fracture-forming effect, and improve the permeability, but also reduce the reservoir damage caused by the leakage. At present, the optimal design of hydraulic fracturing parameters mainly uses numerical simulation methods to adjust the number, length, spacing, and conductivity of fractures, so as to determine the amount of fracturing fluid [18–21]. Usually, the numerical simulation method does not fully consider the flowback of fracturing fluid after hydraulic fracturing. When the flowback effect is not good, the fluid leakage will cause damage to the reservoir, especially related to the impact of fluid migration in the reservoir. Specially, in the process of CBM development in the southern Qinshui Basin by PetroChina Huabei Oilfield Company, the scale of hydraulic fracturing experienced a change from small to large, and the amount of fracturing fluid increased from 300 m³ to 1000 m³, as shown in Table 1. However, it was found that the fracture length and stimulation effect did not increase with the increase of fracturing scale, but large-scale fracturing resulted in more fracturing fluid leaking. During the development process of the Zhengzhuang (ZZ) block, the differences in geological parameters within the block were not considered, and all vertical wells have adopted the same hydraulic fracturing scale, resulting in large differences in gas production of single wells in the block [22].

Table 1. Fracturing fluid volume development stage.

Stage	Time (Year)	Fracturing Fluid Volume (m ³)
I	2006–2007	370–420
II	2008–2009	550–600
III	2010–2011	650–700
IV	2013–2014	800–1000

In this paper, we aim to better clarify whether different FFVs have an impact on gas production, and design the amount of fracturing fluid that matches the geological conditions. By analyzing the production data of 1238 wells in the Fanzhuang (FZ) block and ZZ block, the influence of different FFV on the gas production was studied, the FFV for optimal gas production under the different ratios of critical desorption pressure to the reservoir pressure ($R_{c/T}$) was discussed, and the effect of water block damage caused by fluid leakage on gas production was clarified. The research results can provide some insights into the optimal design of hydraulic fracturing parameters for CBM reservoirs.

2. Geological Setting

The Qinshui Basin, located in southeastern Shanxi Province (Figure 1a), is a typical example of the successful development of high-rank coal in China [23]. The FZ block and ZZ block are located in the southern Qinshui Basin (Figure 1b). The study area consists of the Pennsylvanian Benxi (C₂b) and Taiyuan (C₂t) Formations, the Permian Shanxi

(P_{1s}), Xiashihezi (P_{1x}), Shangshihezi (P_{2s}) and Shiqianfeng (P_{2sh}) Formations, and Triassic deposits. The main coal-bearing strata are the Shanxi and Taiyuan Formations, and the No.3 coal seam of the Shanxi Formation is stably distributed in the whole area and is the main layer for CBM development in the study area [24–26].

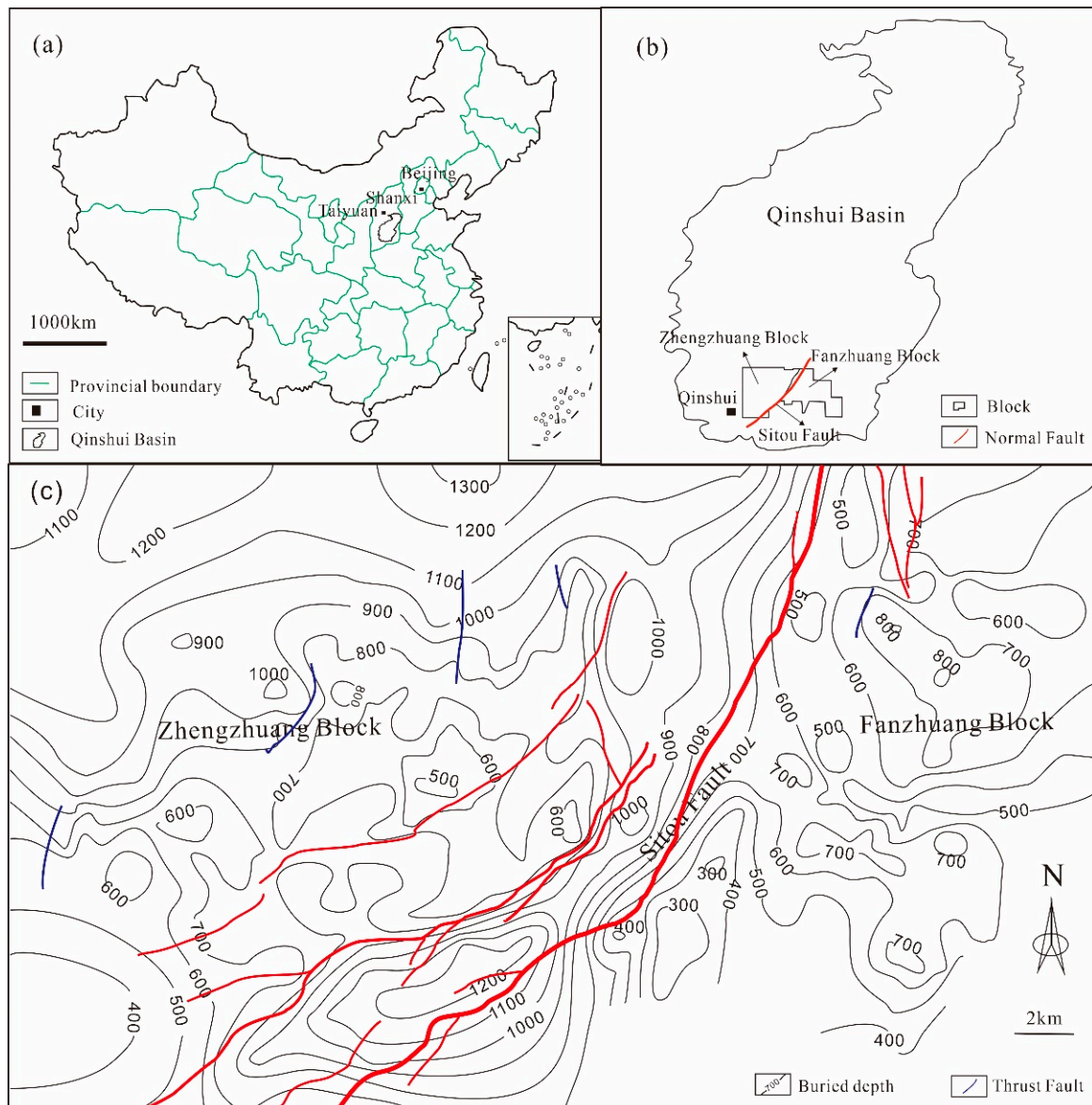


Figure 1. (a) Location of the Qinshui Basin in China; (b) location of development block in the southern Qinshui Basin; (c) the buried depth of the No.3 coal seam.

The FZ block and ZZ block are bounded by the Sitou Fault. The ZZ block is situated west of the fault, and the FZ block is located east of the fault [27–29]. The stratigraphic structure of the study area is relatively complex. Local folds and faults are relatively developed, and the regional structural form is mainly distributed in the north-northeast, and the stratigraphic dip is 3° to 8° . The thickness of the No. 3 coal seam ranges from 5 to 7 m, and its burial depth varies between 300 and 1200 m (Figure 1c). The vitrinite reflectance ($R_{o,max}$, %) varies between 3.1% and 3.9%, and the gas content is between 14 and $30 \text{ m}^3/\text{t}$. The reservoir permeability is generally lower than 1 mD, with an average of 0.27 mD [30–32].

3. Methods

In order to analyze the influence of FFV on gas production in the southern Qinshui Basin, the production data of 1238 CBM wells in FZ block and ZZ block since 2006 were collected and analyzed. These wells all use conventional hydraulic fracturing fluid. The fracturing fluid is potassium chloride solution with a concentration of 1%, and the FFV is between 200–1000 m³. After the fracturing operation, the well is shut in, and the fracturing fluid is almost completely leaked into the reservoir. The basic data collected include FFV, critical desorption pressure, reservoir pressure, $R_{c/r}$, and peak gas production (PGP). Among them, the critical desorption pressure is the bottom hole flow pressure at the initial gas desorption during the CBM drainage process; the $R_{c/r}$ is the ratio of the critical desorption pressure to the reservoir pressure; the PGP is the maximum daily production after the first hydraulic fracturing stimulation.

In this work, one-way analysis of variance (ANOVA) was used to analyze the influence of FFV and $R_{c/r}$ on gas production. First, as many as possible FFV and $R_{c/r}$ are grouped, and then the least-significant difference (LSD) method is used to test the significant differences between the different groups, and the adjacent and insignificant groups are merged [33]. The grouping level of FFV and $R_{c/r}$ is actually obtained, which is convenient for multiway ANOVA. Then, the multiway ANOVA on the significant effect of gas production is carried out using the $R_{c/r}$ and FFV grouping level determined after one-way ANOVA, and then the optimal combination that beneficial to gas production is found [34].

In this work, SPSS software is used for ANOVA, the system default significance level α is set at 0.05 and compared with p -value of the test statistic. If the p -value < 0.05, it is considered that the different grouping levels of the independent variable have a significant impact on the dependent variable. F ratio is the test statistic, the F ratio is the between-group variance divided by the within-group variance in a data set. If $F > 1$, there are statistically significant differences between groups, a high F ratio indicates the greater likelihood of statistically significant differences between groups [34].

4. Results

4.1. One-Way ANOVA

Table 2 shows the results of one-way ANOVA on the PGP when the FFV is divided into 8 groups (200–300 m³, 300–400 m³, 400–500 m³, 500–600 m³, 600–700 m³, 700–800 m³, 800–900 m³, and 900–1000 m³). The results show that the amount of fracturing fluid has a significant effect on PGP ($F = 20.35$, $p = 0.000$). Analysis of the pairwise comparison between different groups by the LSD method shows that the difference between the 300–400 m³ and 400–500 m³ groups is not significant, and they are combined into a group of 300–500 m³. Similarly, the 700–800 m³, 800–900 m³, and 900–1000 m³ were combined into a group of 700–1000 m³. The differences between other adjacent groups are significant, and the results show that the effects of different FFV groups on PGP are significantly different. The average PGP when the FFV is divided into 8 groups is shown in Figure 2a.

Table 2. One-way ANOVA results of 8 groups of FFV.

Source	Sum of Squares	df	Mean Square	F	p -Value
Between-group variance	6.98×10^8	7	9.97×10^7	20.35	0.000
Within-group variance	6.03×10^9	1230	4.9×10^6		
Total	6.72×10^9	1237			

df: The degree of freedom (df) of the statistic.

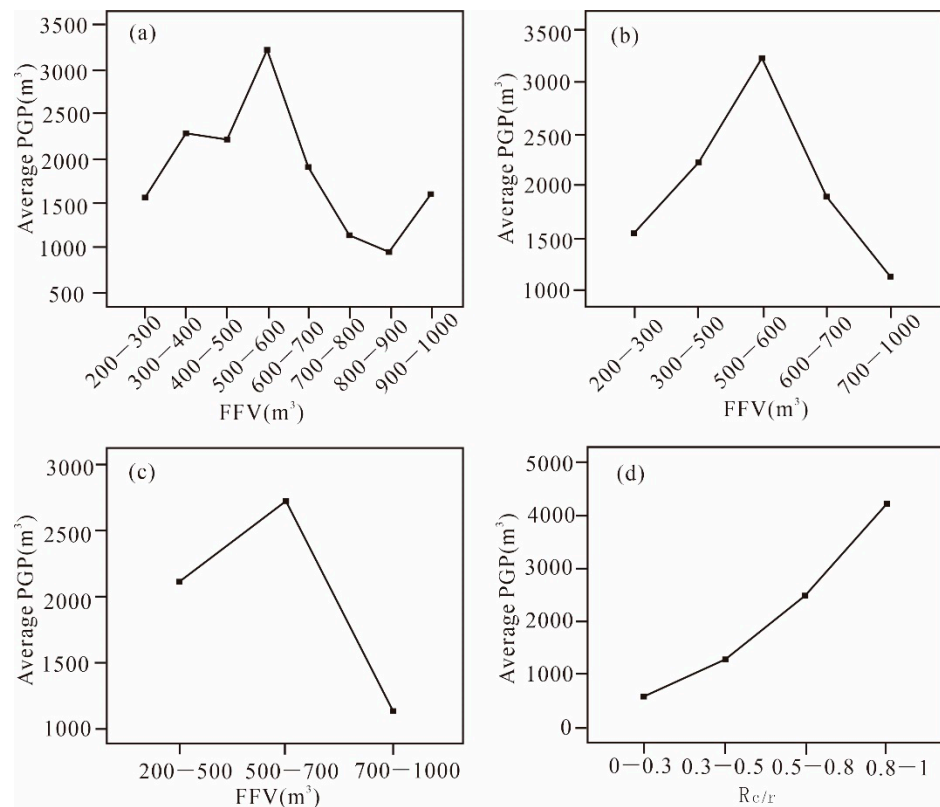


Figure 2. (a) Average PGP when FFV is divided into 8 groups; (b) average PGP when FFV is divided into 5 groups; (c) average PGP when FFV is divided into 3 groups; (d) average PGP when $R_{c/r}$ is divided into 4 groups.

Table 3 shows the results of one-way ANOVA on the PGP when the FFV is divided into 5 groups (200–300 m³, 300–500 m³, 500–600 m³, 600–700 m³, and 700–1000 m³). The results show that the amount of fracturing fluid has a significant effect on the PGP ($F = 35.1$, $p = 0.000$). Figure 2b shows that with the increase of FFV, the average PGP first increases and then decreases. When the FFV is 500–600 m³, the average PGP is the largest, and when the FFV exceeds 500–600 m³, the average PGP shows a rapid downward trend.

Table 3. One-way ANOVA results of 5 groups of FFV.

Source	Sum of Squares	df	Mean Square	F	<i>p</i> -Value
Between-group variance	6.86×10^8	4	1.72×10^8	35.1	0.000
Within-group variance	6.04×10^9	1233	4.9×10^6		
Total	6.72×10^9	1237			

df: The degree of freedom (df) of the statistic.

Table 4 shows the results of one-way ANOVA on the PGP when the FFV is divided into 3 groups (200–500 m³, 500–700 m³, and 700–1000 m³). The results show that the amount of fracturing fluid has a significant effect on PGP ($F = 54.6$, $p = 0.000$). The LSD method analyzes the pairwise comparison between the three different grouping levels, and the results show that the differences between the groups are significant. It can be known from Figure 2c that when the FFV is 200–500 m³, the average PGP is 2136 m³; when the FFV is 500–700 m³, the average PGP is 2795 m³; and when the FFV is 700–1000 m³, the average PGP dropped rapidly to only 1121 m³.

Table 4. One-way ANOVA results of 3 groups of FFV.

Source	Sum of Squares	df	Mean Square	F	p-Value
Between-group variance	5.46×10^8	2	2.73×10^8	54.6	0.000
Within-group variance	6.18×10^9	1235	5×10^6		
Total	6.72×10^9	1237			

df: The degree of freedom (df) of the statistic.

The one-way ANOVA process of $R_{c/r}$ on gas production is shown in Table 5, which shows that $R_{c/r}$ has a significant impact on gas production when $R_{c/r}$ is divided into 10, 7, and 6 groups. Table 6 shows the results of one-way ANOVA on PGP when the $R_{c/r}$ is divided into 4 groups (0–0.3, 0.3–0.5, 0.5–0.8 and 0.8–1). The results showed that the $R_{c/r}$ had a significant impact on the PGP ($F = 111.53$, $p = 0.000$). The results of pairwise comparison between different groups by the LSD method showed that the differences in PGP between the four different grouping levels were significant. Figure 2d shows that the average PGP is positively correlated with the $R_{c/r}$.

Table 5. F and p-value of one-way ANOVA for different groups of $R_{c/r}$.

Variable	Number of Grouping Levels	Grouping Level	F	p-Value
$R_{c/r}$	10	0–0.1, 0.1–0.2, 0.2–0.3, 0.3–0.4, 0.4–0.5, 0.5–0.6, 0.6–0.7, 0.7–0.8, 0.8–0.9, 0.9–1	42.2	0.000
	7	0–0.3, 0.3–0.4, 0.4–0.5, 0.5–0.6, 0.6–0.8, 0.8–0.9, 0.9–1	64.9	0.000
	6	0–0.3, 0.3–0.4, 0.4–0.5, 0.5–0.8, 0.8–0.9, 0.9–1	77.1	0.000

Table 6. One-way ANOVA results of 4 groups of $R_{c/r}$.

Source	Sum of Squares	df	Mean Square	F	p-Value
Between-group variance	1.48×10^9	3	4.74×10^8	111.53	0.000
Within-group variance	5.24×10^9	1234	4.25×10^6		
Total	6.72×10^9	1237			

df: The degree of freedom (df) of the statistic.

One-way ANOVA shows that both the FFV and $R_{c/r}$ have a significant impact on the gas production. Combined with the actual situation, the FFV is divided into 3 groups and the $R_{c/r}$ is divided into 4 groups for multiway ANOVA, as shown in Table 7.

Table 7. Multiway ANOVA variable grouping level table.

Variable	Number of Grouping Levels	Grouping Level	Number of Wells	Total Number of Wells
$R_{c/r}$	4	0–0.3	231	1238
		0.3–0.5	484	
		0.5–0.8	381	
		0.8–1	142	
FFV	3	200–500 m ³	459	1238
		500–700 m ³	259	
		700–1000 m ³	520	

df: The degree of freedom (df) of the statistic.

4.2. Multiway ANOVA

The Levene's test results [$F(11, 1226) = 23.76$, $p = 0.000$] of the multiway ANOVA of the $R_{c/r}$ and FFV can show that the overall variance of the samples in each group is

homogeneous, which meets the precondition of the variance test. Table 8 shows that the model used for the multiway ANOVA was statistically significant ($F = 40.2, p = 0.000$). The interaction between $R_{c/r}$ and FFV had a very significant impact on PGP ($F = 7.42, p = 0.000$).

Table 8. Multiway ANOVA results of $R_{c/r}$ and FFV.

Source	Sum of Squares	df	Mean Square	F	p-Value
Correction model	1.78×10^9	11	1.62×10^8	40.2	0.000
$R_{c/r}$	1.05×10^9	3	3.49×10^8	86.6	0.000
FFV	5.68×10^7	2	2.84×10^7	7.05	0.001
$R_{c/r}$:FFV	1.79×10^8	6	2.99×10^7	7.42	0.000
Error	4.94×10^9	1226	4.03×10^6		
Total	6.72×10^9	1237			

df: The degree of freedom (df) of the statistic.

The multiway ANOVA shows that when the FFV is constant, the larger the $R_{c/r}$, the better the gas production, and the $R_{c/r}$ have a significant contribution to the gas production. When the $R_{c/r}$ is constant, the amount of fracturing fluid is different, and the gas production is also different. The specific performance is as follows: (a) when $R_{c/r} < 0.5$, the gas production is negatively correlated with the amount of fracturing fluid. when $R_{c/r}$ is 0–0.3, the FFV is 700–1000 m³ and the gas production decreases rapidly; when $R_{c/r}$ is 0.3–0.5, the FFV is 500–700 m³ and the gas production decreases rapidly. (b) when $R_{c/r} > 0.5$, the gas production increases first and then decreases with the increase of the FFV, but there are differences. When $R_{c/r}$ is 0.5–0.8, the gas production when the FFV is 700–1000 m³ is less than that when the FFV is 200–500 m³. When $R_{c/r}$ is 0.8–1, the gas production when the FFV is 700–1000 m³ is greater than that when the FFV is 200–500 m³. In short, the gas production decreases when the FFV is 700–1000 m³, indicating that excessive FFV is not conducive to the increase of gas production (Figure 3).

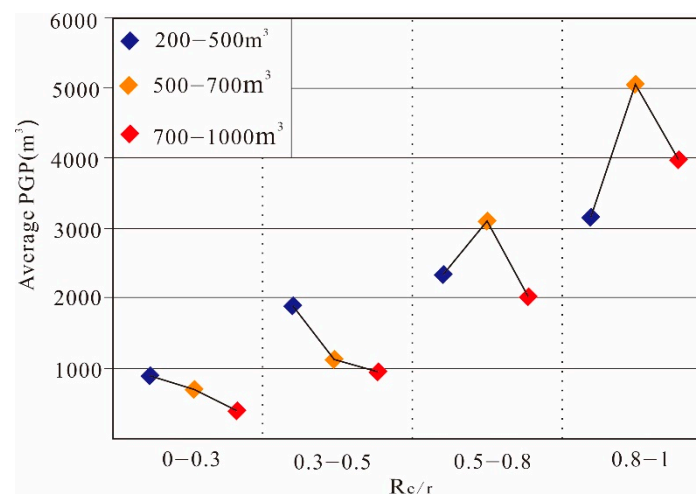


Figure 3. The average peak gas production when $R_{c/r}$ interacts with FFV.

5. Discussion

5.1. Intrusion and Retention of Fracturing Fluid

The process of hydraulic fracturing of CBM wells is the process of intrusion of fracturing fluid into pores and fractures of coal seams. The schematic diagram of fluid distribution in pores and fractures before hydraulic fracturing is shown in Figure 4a. The water intrusion process is mainly affected by injection pressure (P_d), imbibition capillary force (P_c), viscous resistance (P_n), fluid resistance (P_f), and gas pressure (P_g) in the coal seam. It is generally considered that P_d and P_c are the main driving forces [35,36]. When the coal reservoir is saturated with gas and contains more free methane gas, P_g is also a non-negligible

resistance to prevent water migration in pores [37,38]. Therefore, for the fluid migrating in the pores and fractures of coal seams during the water invasion process, the pressure difference (ΔP_i) across the pores is:

$$\Delta P_i = P_d + P_c - P_n - P_f - P_g \quad (1)$$

$$P_c = \frac{2\delta \cos \theta}{r} \quad (2)$$

where σ is the interfacial tension between the solution and the air, N/m; θ is the contact angle between the solution and coal, ($^\circ$); r is the radius of the pore, m.

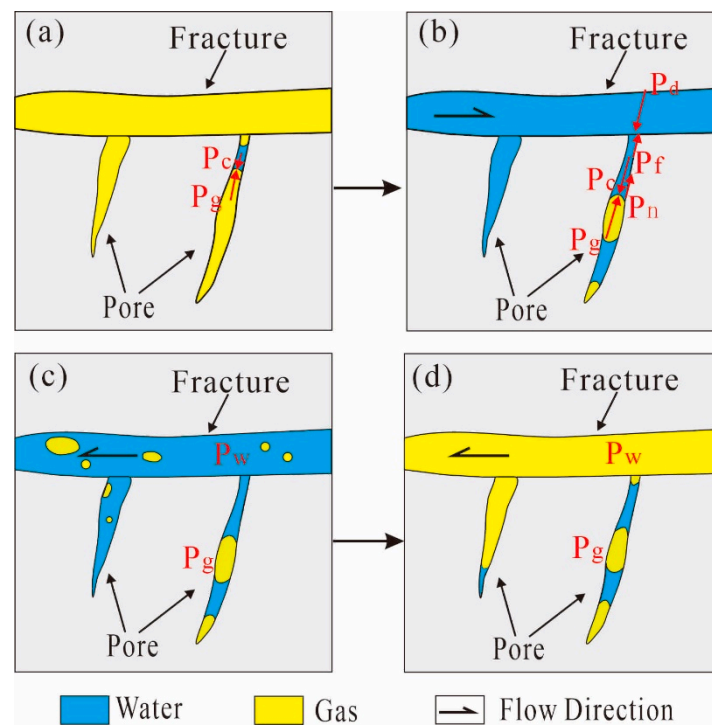


Figure 4. (a) Fluid distribution in pores and fractures before hydraulic fracturing; (b) fluid distribution in pores and fractures after hydraulic fracturing; (c) fluid distribution in pores and fractures at the early stage of drainage; (d) fluid distribution in pores and fractures at the later stage of drainage.

When ΔP_i is >0 , water intrusion occurs. The water retained in the pores may fill the pores, or may form multi-level and intermittent water columns (Figure 4b).

The water intrusion experiments in coal pillars show that water intrusion occurs simultaneously in micropore-transition pores, mesopores, macropores and fractures, and the water intrusion rate decreases sequentially. The speed of water intrusion in the micropore-transition pore is mainly determined by the capillary force of imbibition; the more complex the pore structure, the smaller the degree of water intrusion, and the more difficult it is to flow back after water intrusion. The water saturation of pores and fractures increased with the increase of injection time and inlet pressure during the water invasion process [39].

In the practice of hydraulic fracturing, with the increase of the fracturing scale, the injection rate and pressure need to be increased accordingly. In this way, the amount of fracturing fluid invading into the pores also increases, and the radius of the pores that can be invaded is smaller, and more fracturing fluid enters the complex pores and micropores. Therefore, if the scale of hydraulic fracturing is too large, the more fracturing fluid that is leaked and retained in the pores and fractures, and the residual fracturing fluid will affect the gas production [40]. As shown in Figure 3, when the amount of fracturing fluid is 700–1000 m³, the average PGP decreases compared with that when the amount of fracturing fluid is 500–700 m³, and more external liquid stays in the pores and fractures of the coal.

5.2. Fluid Migration and Water Block Damage during Drainage

At the early stage of CBM well drainage, there is saturated water in the pores and fissures. As the water in the fracture is drained first, the fluid pressure in the fracture will decrease and the gas begins to desorb (Figure 4c). After the water in the fracture is drained out, some of the water in the pore does not migrate with the water in the fracture, but stays in the pore (Figure 4d). According to the principle of gas-liquid two-phase fluid flow, it can be known that the fluid in the pore mainly considers the two-phase flow driven by the pressure difference [41]. The pressure difference for liquid column migration in the pore is [13,42]:

$$\Delta P_o = P_g - P_c - P_w - P_f - G \quad (3)$$

where P_g is the gas pressure in the pore; P_w is the fluid pressure in the fracture; and G is the gravity of the liquid column in the pore.

P_g is the main driving force for the liquid column migration in the pore, and P_c and P_w are the main resistances. When the pore radius is small enough and the liquid column is short enough, P_f and G can be ignored. When $\Delta P_o = 0$, the fluid in the pore does not migrate (Figure 5a). As the fluid in the fracture migrates out, P_w will decrease, the pressure drop will be transferred to the pore, and part of the adsorbed gas will be desorbed from the pore, and P_g will increase. When $\Delta P_o > 0$, the liquid column migrates to the fracture. At this time, the fluid pressure balance in the pore is destroyed, and the gas at the bottom of the pore will push the liquid column at the bottom upward until a new balance is reached (Figure 5b). With the progress of drainage, the pressure drop is effectively transferred to the internal pores, and more gas is desorbed. When the flow resistance of the liquid column can be overcome, the gas will break through the constraints of the liquid and migrate out. At this time, the pores and fractures are fully connected (Figure 5c). In this process, the part of the liquid column that cannot overcome its flow resistance is bound in the pores, blocking the pores, affecting the migration of gas, and forming water block damage.

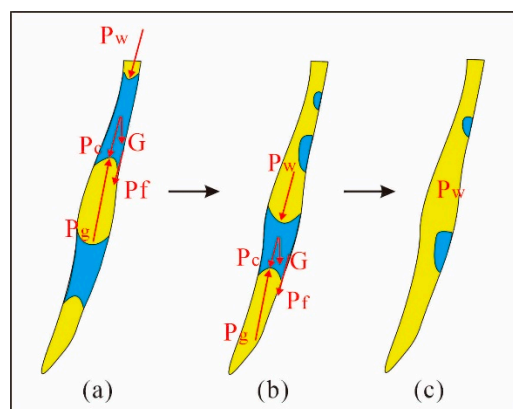


Figure 5. (a) Schematic diagram of the force when the fluid in the pores does not migrate; (b) schematic diagram of the fluid in the pores in a new balance state; (c) schematic diagram when pores and fractures are fully connected.

The gas flooding experiment also showed that the water block damage of macropores and fractures can be relieved, and the water block of mesopores can be partially relieved, while the water in micropores and transition pores was difficult to displace [39,43,44]. In actual production, a large amount of fracturing fluid invades into the pores, and there is no additional driving force during the drainage process, and it will be more difficult for the fracturing fluid to be completely discharged from the micropores and transition pores. Therefore, this part of water must rely on the driving force of the gas in the pores to be discharged.

5.3. Mechanism of FFV Affecting Gas Production

It can be seen from the above analysis that water block mainly comes in two ways: (1) during the fracturing process, a large amount of fracturing fluid intrudes into the pores and fractures, and is trapped by capillary force; (2) in the process of drainage, the driving force of the gas in the pore is not enough to overcome the resistance of its migration, and the fracturing fluid retained in the pore cannot be discharged back. According to the Hagen–Poiseuille law, the volume of the fracturing fluid discharged from the pores against the capillary resistance is [45]:

$$Q = \frac{\pi r^4 \Delta P_o}{8\mu L} \quad (4)$$

where Q is the volume of fracturing fluid discharged, m^3 ; r is the radius of the pore, m ; μ is the dynamic viscosity, $Pa \cdot s$; L is the length of the liquid column, m .

Take the derivative of Equation (4) as

$$\frac{dL}{dt} = \frac{r^2 \Delta P_o}{8\mu L} \quad (5)$$

By the integral of Equation (5), it can be obtained that the time (t) for the liquid column of length (L) to flow back from the pores is

$$t = \frac{4\mu L^2}{\Delta P_o r^2} \quad (6)$$

Substitute Equation (3) into Equation (6):

$$t = \frac{4\mu L^2}{(P_g - P_c - P_w - P_f - G)r^2} \quad (7)$$

When the scale of hydraulic fracturing fluid increases, the amount of invading fluid in pores increases, the length of the liquid column (L) increases, and the radius (r) of the pores that can be invaded becomes smaller; at the same time, the P and G of the liquid column will have to be considered, increasing the resistance and time for the fluid to move out, making it easier to cause water block [37].

According to the analysis of the microseismic fracture monitoring report of CBM wells in the study area, the FFV has no significant effect on the length of the fracture, and the length of the fracture does not increase with the increase of the FFV (Figure 6). The correlation between gas production and fracture length is also not obvious (Figure 7). It can be seen that increasing the scale of fracturing has not always brought positive effects on gas production [22]. From the one-way ANOVA of FFV and PGP (Figure 2), it can be seen that with the increase of FFV, the PGP increases first and then decreases. Within a certain scale, increasing the amount of fracturing fluid has a positive effect on gas production. When it exceeds a certain scale, it will have a negative effect on gas production. This is because excess fracturing fluid does not play a role in creating fractures and increasing reservoir connectivity. The excess fracturing fluid is leaked into the coal reservoir or surrounding rock along the pore and fracture channels, and the positive effect is not as great as the negative effect of water block caused by excessive fracturing fluid staying in the reservoir [46]. Therefore, the negative impact of FFV on gas production is mainly reflected in the water block damage caused to the reservoir.

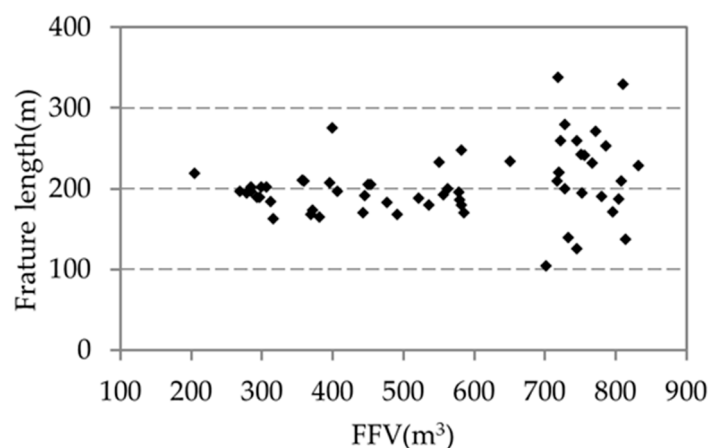


Figure 6. Diagram of FFV and hydraulic fracturing fracture length.

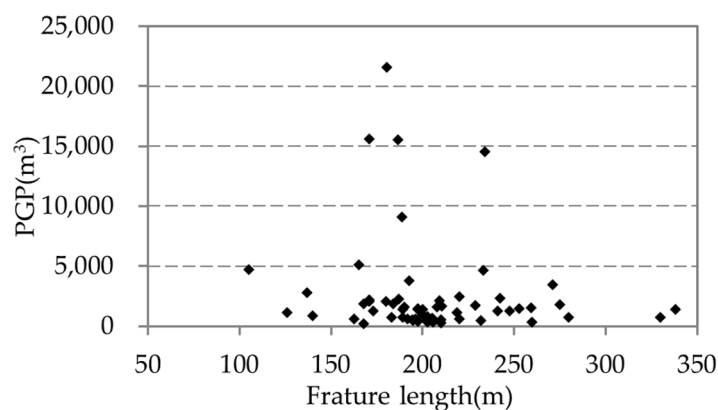


Figure 7. Diagram of hydraulic fracturing fracture length and PGP.

It can be seen from Equation (7) that the greater the ΔP_o , the greater the fluid resistance that can be overcome. Therefore, under different reservoir conditions, the degree of difficulty in releasing the water block is also different. Lyu et al. [38] and Lu et al. [42] showed that water block did not occur when the differential pressure driving force was greater than the resistance. The larger the $R_{c/r}$ value, the better the fluid drainage index of the reservoir, which was more conducive to the desorption of gas, resulting in high production [47]. The $R_{c/r}$ value can represent the gas saturation to a certain extent. Higher gas saturation leads to higher desorption pressure and is beneficial for early gas production, leading to greater total gas production [48,49]. It can be seen that the larger the $R_{c/r}$ value, the easier the gas desorption, the greater the pressure of gas in the pore, and the greater the driving force of liquid migration in the pore. Therefore, when the $R_{c/r}$ increases, it becomes easier for the water in the pores to be displaced out.

As shown in Figure 3, when $R_{c/r} > 0.5$, the gas production with the FFV of 500–700 m^3 is better than that with the FFV of 200–500 m^3 , indicating that the positive effect of increasing the FFV on the reservoir is greater than the water block damage to the reservoir. When the amount of fracturing fluid increases to 700–1000 m^3 , the gas production decreases, indicating that the damage of the water block caused by increasing the volume of fracturing fluid is greater than the positive effect caused by increasing the volume of fracturing fluid. In particular, when $R_{c/r}$ is 0.5–0.8, the gas production with the FFV of 700–1000 m^3 is smaller than that with the FFV of 200–500 m^3 , implying that the negative effect of excessively increasing the amount of fracturing fluid is greater, and more water blocks are not released. When $R_{c/r}$ is 0.8–1, the gas production with the FFV of 700–1000 m^3 is higher than that of the FFV of 200–500 m^3 , indicating that the positive effect brought by the large FFV is greater than the negative effect. The water block is easier to be eliminated when the

$R_{c/r}$ is 0.8–1 than when the $R_{c/r}$ is 0.5–0.8. When $R_{c/r} < 0.5$, the gas production will be less when the FFV is increased, which indicates that the fracturing fluid enters the pores and is difficult to be displaced, which is more likely to cause water block damage to the reservoir. Therefore, the smaller the $R_{c/r}$ value, the larger the FFV, and the more serious the water block damage.

5.4. The Uncertainty or Limitation of This Study

There are many factors affecting the production of CBM [32,50–53]. This paper illustrates that the amount of fracturing fluid is also one of the factors affecting the production of gas through the ANOVA of production data. This paper selects the $R_{c/r}$ and FFV for multivariate ANOVA, and proposes that the design of FFV can be based on the $R_{c/r}$ in the study area. The combination of other geological factors and FFV may also affect gas production and multivariate ANOVA of other geological parameters, and FFV may be attempted later. In this paper, the coal samples in the study area are not used for the analysis of water intrusion, drainage, and water block in pores and fractures, and the experiment of Li et al. [40] is cited for illustration. The data in this paper are from the FZ block and ZZ block in Qinshui Basin, which is a high-rank coal, so the applicability of the optimal combination and the reference of FFV parameter design are only applicable to this block.

6. Conclusions

- (1) One-way ANOVA shows that FFV has a significant effect on gas production. In particular, with the increase of FFV, the gas production increases first and then decreases, and the best gas production is when the FFV is 500–600 m³ in the study area.
- (2) When the $R_{c/r} < 0.5$ (0–0.3 and 0.3–0.5), the gas production is negatively correlated with the FFV. When the $R_{c/r} > 0.5$ (0.5–0.8 and 0.8–1), the gas production increases first and then decreases with the increase of FFV. The best combination for gas production is the $R_{c/r}$ of 0.8–1 and the FFV of 500–700 m³.
- (3) It is found that too much injected fracturing fluid will increase the fluid leakage and lead to the water block damage of coal reservoir, and the increase of the $R_{c/r}$ is conducive to removing the water block damage. Therefore, it is necessary to adapt the optimal amount of fracturing fluid according to the condition of the $R_{c/r}$ in the study area, so as to achieve the best fracturing effect.

Author Contributions: Methodology, writing—original draft, W.C. (Wenwen Chen); data curation, investigation, F.Q. and W.C. (Weiwei Chao); data curation, resources, M.T. and W.C. (Wei Chen); revised and edited the manuscript, X.W. and S.H. All authors have read and agreed to the published version of the manuscript.

Funding: This research was funded by National Science Foundation of China (No. 41972184, No. 42262022 and No. 41902177) and Jiangxi Provincial Natural Science Foundation (grant number 20212BAB214030).

Acknowledgments: The authors would like to give their sincere thanks to the teachers in the department for their comments on the revision of the article, and thanks to the former colleagues of PetroChina Huabei Oilfield Company for their valuable comments.

Conflicts of Interest: The authors declare no conflict of interest.

References

1. Xu, B.; Li, X.; Haghghi, M.; Ren, W.; Du, X.; Chen, D.; Zhao, Y. Optimization of hydraulically fractured well configuration in anisotropic coal-bed methane reservoirs. *Fuel* **2013**, *107*, 859–865. [[CrossRef](#)]
2. Yuan, B.; Wood, D.A.; Yu, W. Stimulation and hydraulic fracturing technology in natural gas reservoirs: Theory and case studies (2012–2015). *J. Nat. Gas Sci. Eng.* **2015**, *26*, 1414–1421. [[CrossRef](#)]
3. Yan, Q.; Lemanski, C.; Karpyn, Z.T.; Ayala, L.F. Experimental investigation of shale gas production impairment due to fracturing fluid migration during shut-in time. *J. Nat. Gas Sci. Eng.* **2015**, *24*, 99–105. [[CrossRef](#)]
4. Yuan, X.; Yao, Y.; Liu, D.; Pan, Z. Spontaneous imbibition in coal: Experimental and model analysis. *J. Nat. Gas Sci. Eng.* **2019**, *67*, 108–121. [[CrossRef](#)]

5. Naik, S.; You, Z.; Bedrikovetsky, P. Rate enhancement in unconventional gas reservoirs by wettability alteration. *J. Nat. Gas Sci. Eng.* **2015**, *26*, 1573–1584. [[CrossRef](#)]
6. Su, X.; Wang, Q.; Song, J.; Chen, P.; Yao, S.; Hong, J.; Zhou, F. Experimental study of water blocking damage on coal. *J. Pet. Sci. Eng.* **2017**, *156*, 654–661. [[CrossRef](#)]
7. Huang, Q.; Liu, S.; Cheng, W.; Wang, G. Fracture permeability damage and recovery behaviors with fracturing fluid treatment of coal: An experimental study. *Fuel* **2020**, *282*, 118809. [[CrossRef](#)]
8. Chang, Y.; Yao, Y.; Liu, D.; Liu, Y.; Cui, C.; Wu, H. Behavior and mechanism of water imbibition and its influence on gas permeability during hydro-fracturing of a coalbed methane reservoir. *J. Pet. Sci. Eng.* **2022**, *208*, 109745. [[CrossRef](#)]
9. Bahrami, H.; Rezaee, R.; Clennell, B. Water blocking damage in hydraulically fractured tight sand gas reservoirs: An example from Perth Basin, Western Australia. *J. Pet. Sci. Eng.* **2012**, *88–89*, 100–106. [[CrossRef](#)]
10. Yang, S.; Wen, G.; Yan, F.; Li, H.; Liu, Y.; Wu, W. Swelling characteristics and permeability evolution of anthracite coal containing expansive clay under water-saturated conditions. *Fuel* **2020**, *279*, 118501. [[CrossRef](#)]
11. Li, X.; Kang, Y. Effect of fracturing fluid immersion on methane adsorption/desorption of coal. *J. Nat. Gas Sci. Eng.* **2016**, *34*, 449–457. [[CrossRef](#)]
12. Lu, W.; Huang, B.; Zhao, X. A review of recent research and development of the effect of hydraulic fracturing on gas adsorption and desorption in coal seams. *Adsorpt. Sci. Technol.* **2019**, *37*, 509–529. [[CrossRef](#)]
13. Wang, Z.; Liu, S.; Qin, Y. Coal wettability in coalbed methane production: A critical review. *Fuel* **2021**, *303*, 121277. [[CrossRef](#)]
14. Meng, Y.; Li, Z.; Lai, F. Evaluating the filtration property of fracturing fluid and fracture conductivity of coalbed methane wells considering the stress-sensitivity effects. *J. Nat. Gas Sci. Eng.* **2020**, *80*, 103379. [[CrossRef](#)]
15. Guo, J.; Liu, Y. A comprehensive model for simulating fracturing fluid leakoff in natural fractures. *J. Nat. Gas Sci. Eng.* **2014**, *21*, 977–985. [[CrossRef](#)]
16. Guo, J.; Liu, Y. Opening of natural fracture and its effect on leakoff behavior in fractured gas reservoirs. *J. Nat. Gas Sci. Eng.* **2014**, *18*, 324–328. [[CrossRef](#)]
17. Wu, C.; Zhang, X.; Wang, M.; Zhou, L.; Jiang, W. Physical simulation study on the hydraulic fracture propagation of coalbed methane well. *J. Appl. Geophys.* **2018**, *150*, 244–253. [[CrossRef](#)]
18. Jiang, T.; Zhang, J.; Wu, H. Experimental and numerical study on hydraulic fracture propagation in coalbed methane reservoir. *J. Nat. Gas Sci. Eng.* **2016**, *35*, 455–467. [[CrossRef](#)]
19. Jahandideh, A.; Jafarpour, B. Optimization of hydraulic fracturing design under spatially variable shale fracability. *J. Pet. Sci. Eng.* **2016**, *138*, 174–188. [[CrossRef](#)]
20. Zhao, J.; Zhao, J.; Hu, Y.; Zhang, S.; Huang, T.; Liu, X. Numerical simulation of multistage fracturing optimization and application in coalbed methane horizontal wells. *Eng. Fract. Mech.* **2020**, *223*, 106738. [[CrossRef](#)]
21. Song, H.; Du, S.; Yang, J.; Zhao, Y.; Yu, M. Evaluation of hydraulic fracturing effect on coalbed methane reservoir based on deep learning method considering physical constraints. *J. Pet. Sci. Eng.* **2022**, *212*, 110360. [[CrossRef](#)]
22. Zhu, Q.; Zuo, Y.; Yang, Y. How to solve the technical problems in the CBM development: A case study of a CBM gas reservoir in the southern Qinshui Basin. *Nat. Gas Ind.* **2015**, *35*, 106–109. [[CrossRef](#)]
23. Chen, S.; Tang, D.; Tao, S.; Xu, H.; Li, S.; Zhao, J.; Cui, Y.; Li, Z. Characteristics of in-situ stress distribution and its significance on the coalbed methane (CBM) development in Fanzhuang-Zhengzhuang Block, Southern Qinshui Basin, China. *J. Pet. Sci. Eng.* **2018**, *161*, 108–120. [[CrossRef](#)]
24. Su, X.; Li, X.; Li, S.; Zhao, M.; Song, Y. Geology of coalbed methane reservoirs in the Southeast Qinshui Basin of China. *Int. J. Coal Geol.* **2005**, *62*, 197–210. [[CrossRef](#)]
25. Zhang, J.; Liu, D.; Cai, Y.; Pan, Z.; Yao, Y.; Wang, Y. Geological and hydrological controls on the accumulation of coalbed methane within the No. 3 coal seam of the southern Qinshui Basin. *Int. J. Coal Geol.* **2017**, *182*, 94–111. [[CrossRef](#)]
26. Han, W.; Wang, Y.; Li, Y.; Ni, X.; Wu, X.; Wu, P.; Zhao, S. Recognizing fracture distribution within the coalbed methane reservoir and its implication for hydraulic fracturing: A method combining field observation, well logging, and micro-seismic detection. *J. Nat. Gas Sci. Eng.* **2021**, *92*, 103986. [[CrossRef](#)]
27. Chen, Y.; Liu, D.; Yao, Y.; Cai, Y.; Chen, L. Dynamic permeability change during coalbed methane production and its controlling factors. *J. Nat. Gas Sci. Eng.* **2015**, *25*, 335–346. [[CrossRef](#)]
28. Zhao, X.; Yang, Y.; Sun, F.; Wang, B.; Zuo, Y.; Li, M.; Shen, J.; Mu, F. Enrichment mechanism and exploration and development technologies of high coal rank coalbed methane in south Qinshui Basin, Shanxi Province. *Pet. Explor. Dev.* **2016**, *43*, 332–339. [[CrossRef](#)]
29. Shi, J.; Zeng, L.; Zhao, X.; Zhao, Y.; Wang, J. Characteristics of natural fractures in the upper Paleozoic coal bearing strata in the southern Qinshui Basin, China: Implications for coalbed methane (CBM) development. *Mar. Pet. Geol.* **2020**, *113*, 104152. [[CrossRef](#)]
30. Cai, Y.; Liu, D.; Yao, Y.; Li, J.; Qin, Y. Geological controls on prediction of coalbed methane of No. 3 coal seam in Southern Qinshui Basin, North China. *Int. J. Coal Geol.* **2011**, *88*, 101–112. [[CrossRef](#)]
31. Zhang, J.; Liu, D.; Cai, Y.; Yao, Y.; Ge, X. Carbon isotopic characteristics of CH₄ and its significance to the gas performance of coal reservoirs in the Zhengzhuang area, Southern Qinshui Basin, North China. *J. Nat. Gas Sci. Eng.* **2018**, *58*, 135–151. [[CrossRef](#)]
32. Shen, J.; Qin, Y.; Li, Y.; Yang, Y.; Ju, W.; Yang, C.; Wang, G. In situ stress field in the FZ Block of Qinshui Basin, China: Implications for the permeability and coalbed methane production. *J. Pet. Sci. Eng.* **2018**, *170*, 744–754. [[CrossRef](#)]

33. Lizasoain, L.; Joaristi, L. *Management and Data Analysis with SPSS*; Paraninfo S.A.: Madrid, Spain, 2003; p. 480.
34. Harris, J.; Sheean, P.; Gleason, P.; Bruemmer, B.; Boushey, C. Publishing Nutrition Research: A Review of Multivariate Techniques—Part 2: Analysis of Variance. *J. Acad. Nutr. Diet.* **2012**, *112*, 90–98. [[CrossRef](#)]
35. Yao, Y.; Liu, D.; Liu, J.; Xie, S. Assessing the water migration and permeability of large intact bituminous and anthracite coals using NMR relaxation spectrometry. *Transp. Porous Media* **2015**, *107*, 527–542. [[CrossRef](#)]
36. Sun, X.; Yao, Y.; Liu, D.; Zhou, Y. Investigations of CO₂-water wettability of coal: NMR relaxation method. *Int. J. Coal Geol.* **2018**, *188*, 38–50. [[CrossRef](#)]
37. Lyu, S.; Chen, X.; Shah, S.M.; Wu, X. Experimental study of influence of natural surfactant soybean phospholipid on wettability of high-rank coal. *Fuel* **2019**, *239*, 1–12. [[CrossRef](#)]
38. Lyu, S.; Wang, S.; Li, J.; Chen, X.; Chen, L.; Dong, Q.; Zhang, X.; Huang, P. Massive Hydraulic Fracturing to Control Gas Outbursts in Soft Coal Seams. *Rock Mech. Rock Eng.* **2022**, *55*, 1759–1776. [[CrossRef](#)]
39. Li, X.; Fu, X.; Ranjith, P.G.; Fang, Y. Retained water content after nitrogen driving water on flooding saturated high volatile bituminous coal using low-field nuclear magnetic resonance. *J. Nat. Gas Sci. Eng.* **2018**, *57*, 189–202. [[CrossRef](#)]
40. Sharma, M.; Agarwal, S. Impact of liquid loading in hydraulic fractures on well productivity. *J. Pet. Technol.* **2013**, *65*, 162–165. [[CrossRef](#)]
41. Li, X.; Shi, J.; Du, X.; Hu, A.; Chen, D.; Zhang, D. Transport mechanism of desorbed gas in coalbed methane reservoirs. *Pet. Explor. Dev.* **2012**, *39*, 203–213. [[CrossRef](#)]
42. Lu, Y.; Li, H.; Lu, J.; Shi, S.; Wang, G.; Ye, Q.; Li, R.; Zhu, X. Clean up water blocking damage in coalbed methane reservoirs by microwave heating: Laboratory studies. *Process Saf. Environ. Prot.* **2020**, *138*, 292–299. [[CrossRef](#)]
43. Connolly, P.R.J.; Vogt, S.J.; Iglauer, S.; May, E.F.; Johns, M.L. Capillary trapping quantification in sandstones using NMR relaxometry. *Water Resour. Res.* **2017**, *53*, 7917–7932. [[CrossRef](#)]
44. He, F.; Wang, J. Study on the Causes of Water Blocking Damage and Its Solutions in Gas Reservoirs with Microfluidic Technology. *Energies* **2022**, *15*, 2684. [[CrossRef](#)]
45. Liu, D.; Yao, Y.; Yuan, X.; Yang, Y. Experimental evaluation of the dynamic water-blocking effect in coalbed methane reservoir. *J. Petrol. Sci. Eng.* **2022**, *217*, 110887. [[CrossRef](#)]
46. Chen, M.; Bai, J.; Kang, Y.; Chen, Z.; You, L.; Li, X.; Liu, J.; Zhang, Y. Redistribution of fracturing fluid in shales and its impact on gas transport capacity. *J. Nat. Gas Sci. Eng.* **2020**, *86*, 103747. [[CrossRef](#)]
47. Zhao, X.; Yang, Y.; Chen, L.; Yang, Y.; Shen, J.; Chao, W.; Shao, G. Production controlling mechanism and mode of solid-fluid coupling of high rank coal reservoirs. *Acta Pet. Sinic.* **2015**, *36*, 1024–1034. [[CrossRef](#)]
48. Tao, S.; Tang, D.Z.; Xu, H.; Gao, L.J.; Fang, Y. Factors controlling high-yield coalbed methane vertical wells in the Fanzhuang Block, Southern Qinshui Basin. *Int. J. Coal Geol.* **2014**, *134*, 38–45. [[CrossRef](#)]
49. Tao, S.; Pan, Z.; Tang, S.; Chen, S. Current status and geological conditions for the applicability of CBM drilling technologies in China: A review. *Int. J. Coal Geol.* **2019**, *202*, 59–108. [[CrossRef](#)]
50. Moore, T. Coalbed methane: A review. *Int. J. Coal Geol.* **2012**, *101*, 36–81. [[CrossRef](#)]
51. Guo, Q.; Fink, R.; Littke, R.; Zieger, L. Methane sorption behaviour of coals altered by igneous intrusion, South Sumatra Basin. *Int. J. Coal Geol.* **2019**, *214*, 103250. [[CrossRef](#)]
52. Fu, H.; Yan, D.; Su, X.; Wang, J.; Li, Q.; Li, X.; Zhao, W.; Zhang, L.; Wang, X.; Li, Y. Biodegradation of early thermogenic gas and generation of secondary microbial gas in the Tieliekedong region of the northern Tarim Basin, NW China. *Int. J. Coal Geol.* **2022**, *261*, 104075. [[CrossRef](#)]
53. Qin, Y.; Moore, T.; Shen, J.; Yang, Z.; Shen, Y.; Wang, G. Resources and geology of coalbed methane in China: A review. *Int. Geol. Rev.* **2018**, *60*, 777–817. [[CrossRef](#)]